Environmental Noise of VSR4 and Preparing for Advanced Virgo

David R. Miller[1]

[1] *Carleton College, One North College Street, Northfield, Minnesota 55057*

To increase the detector sensitivity of the Virgo interferometer, it is important to identify noise lines in order to mitigate their sources. Using the Noemi and coherence tools, I produced a list of all noise lines between 10 and 100 Hz for VSR4. Advanced Virgo aims to reduce noise line sources by using less noisy cooling fans. I performed measurements of five different cooling fans and found the fan EbmPapst 4890 performed best.

I. INTRODUCTION

When a mass accelerates, it creates a ripple through the fabric of space-time. These ripples are known as gravitational waves. The theory of general relativity predicts the existence of gravitational waves, but they have never been directly observed (only indirectly). Virgo is a scientific experiment in Cascina, Italy attempting to detect gravitational waves using a laser Michelson interferometer. Virgo collaborates with two similar Michelson interferometers in the United States known as LIGO (Laser Interferometer Gravitational-Wave Observatory) and one in Germany known as GEO-600 (German-British Gravitational Wave Detector).

The interferometer at Virgo consists of two orthogonal arms, each of length 3 kilometers. A gravitational wave would stretch one arm of the interferometer while compressing the other such that the distance between free masses within the arms would alternately increase and decrease. The change in distance between the masses is millions of times smaller than an atom, and thus Virgo uses the phenomenon of wave interference to detect such a small variation in length. A beam splitter is used to equally divide the incident laser beam down the two orthogonal arms. The light is then reflected back toward the beam splitter by mirrors at the end of the two arms and enters the detector, consisting of a photodiode. Before reaching the end mirrors, the light first travels through a Fabry-Perot cavity, which, by multiple reflections, extends the travel distance of the light to over 100 kilometers within the 3 kilometer arm, amplifying the distance variation between the masses. In the absence of a gravitational wave, the light entering the detector will undergo destructive interference such that no light reaches the output photodetector [3]. For this reason, the output photodiode signal is referred to as the *dark fringe*. Figure 1 shows a simplified layout of the Virgo interferometer.

When gravitational waves are eventually detected, the analysis of the dark fringe would provide a new image of the universe. This image would be a special one, for it would not be on the electromagnetic spectrum but instead on a brand new gravitational spectrum of viewing the universe. It is as if we are watching the universe using the electromagnetic spectrum, but need the gravitational spectrum to hear the universe [3].

Virgo mirrors are suspended from multi-pendulum structures (10 meters tall) called the Super-attenuators, which guarantee sufficient isolation from the ground vibrations (a factor of 10^{12}) starting at around 10 Hz. The Super-attenuators allow Virgo to reach quality sensitivity in the 10 to 100 Hz region. Nevertheless, noise from external sources can enter the interferometer via complicated paths and deteriorate the sensitivity at certain frequencies. Most noise is the result of numerous electro-mechanical devices (engines, pumps, fans) located around the interferometer which continuously emit vibration noise at almost-constant frequencies (their rotation speed and multiples). The noise polluting the interferometer can appear as a peak at a fixed frequency in the dark fringe signal power spectrum that persists in time, or as a horizontal line in the time-frequency spectrogram of the dark fringe signal; hence the noise is referred to as a *noise line* [2]. Noise lines are classified by their frequency, amplitude, width, and signal to noise ratio (SNR). It is important to identify noise lines and mitigate their sources in order to achieve sufficient detector sensitivity. To identify noise lines, Virgo uses a line-monitoring tool named NoEMi (Noise Event Miner), which analyzes the Dark Fringe and environmental sensors to search for coincidences among the channels. Another similar environmental monitoring tool that Virgo uses is the coherence of the Dark Fringe and environmental channels to again search for coincidences among the channels. In Section 2, I identify noise lines in Virgo's 4^{th} Scientific Run (VSR4) ranging from 10 to 100 Hz using the NoEMi and coherence tools.

One source of noise lines is fans used to cool the electronics within the interferometer. Advanced Virgo plans to reduce the environmental noise from cooling fans by using fans that produce less acoustic noise. I tested five different fans of varying speed and air flow, and present my results in Section 3.

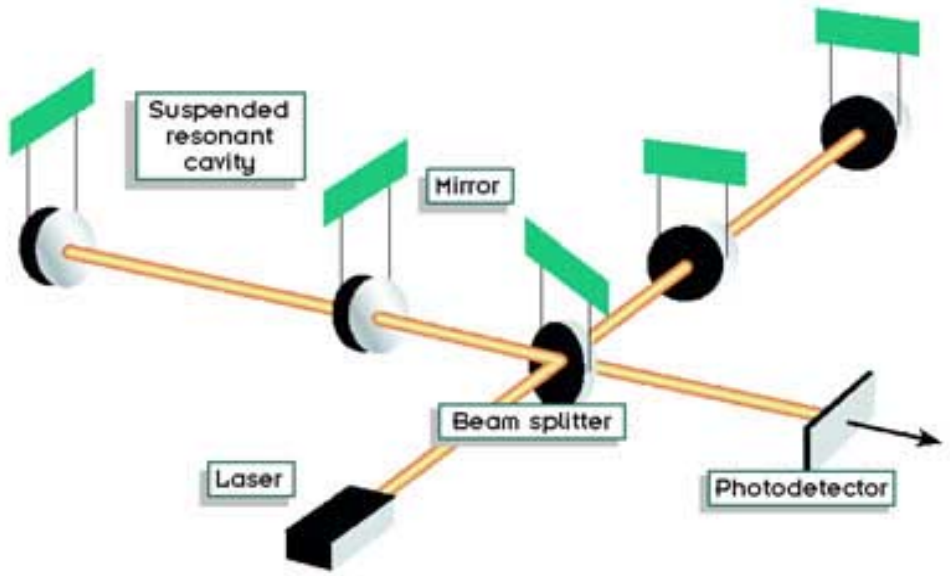

FIG. 1: The scheme of the Virgo Michelson interferometer. The incident light from the laser beam is split down two orthogonal arms. The light travels a distance of over 100 kilometers within the 3 kilometer long arms due to the resonant Fabry-Perot cavity consisting of two highly reflective mirrors. The light then returns to the beam splitter and enters the photodiode detector, where in the absence of a gravitational wave, the light overlaps destructively resulting in no signal in the photodiode detector. A small change in length difference between the two arms, for example caused by a gravitational wave, would result in a light flash in the photodiode.

II. ENVIRONMENTAL NOISE OF VSR4

Virgo started VSR4 on June 3rd, 2011 and expects to conclude VSR4 in September of 2011. A focus of VSR4 is to acquire long, continuous streams of data at high detector sensitivity in frequency regions of known pulsars. Pulsars are rotating neutron stars that are expected to emit gravitational waves at double their rotational speed. Astronomers have detected pulsars spinning in the frequency range from 10 to 100 Hz, in particular, the Vela (22.38 Hz) and the Crab (59 Hz) pulsars that are predicted to emit the strongest gravitational wave signals. Thus, it is crucial to identify noise lines in the VSR4 interferometer noise spectrum between 10 and 100 Hz in order to mitigate their sources to increase detector sensitivity to pulsar gravitational wave signals.

A. Noise Monitoring Tools - Noemi and Coherence

NoEMi is the main tool used by Virgo to identify and track noise lines in the dark fringe. Noemi processes data from the dark fringe on a daily basis, and seeks to identify noise lines by finding coincidence between the dark fringe signal and over a hundred of environmental sensors (i.e. seismometers, magnetometers, microphones, voltage and current probes) strategically placed throughout the interferometer. Noemi uses a sophisticated algorithm implemented for the search of continuous gravitational wave signals to reconstruct the evolution in time of lines [2]. Noemi reports its findings in a database, including the frequency of the noise line, the environmental channels that correlate with the noise line, and a percentage representing the amount of coincidence between the dark fringe and the environmental channel (a greater percentage means greater coincidence). Figure 2 shows a NoEMi plot of the noise lines surrounding the Vela pulsar on July 27, 2011.

To supplement Noemi, Virgo uses the coherence tool. The coherence tool compares the frequency composition of the dark fringe signal to each one of the environmental sensor signals by computing the mathematical coherence function of the two signals for a given time interval and frequency resolution. The coherence reports its findings as a number between 0 and 1, where 0 is no coherence and 1 is complete coherence. Figure 3 shows a plot of the coherence between the dark fringe and a seismometer located in the central building on July 28, 2011. Together, the coherence and NoEMi are effective tools at identifying noise lines in the dark fringe.

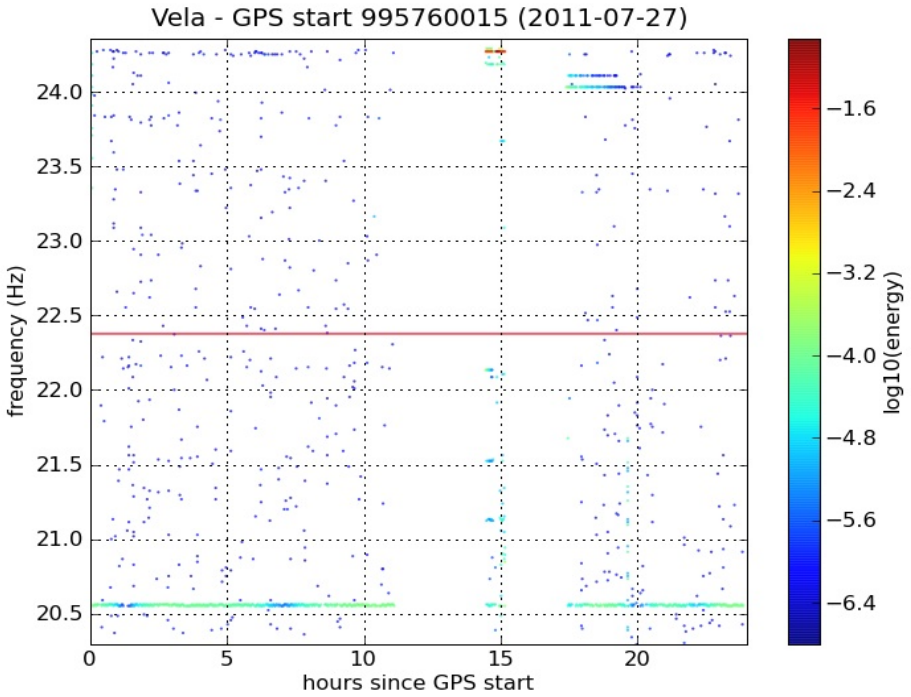

FIG. 2: A NoEMi plot (frequency vs. time) showing the track of lines surrounding the Vela pulsar on July 27, 2011. The red line indicates the expected Vela signal.

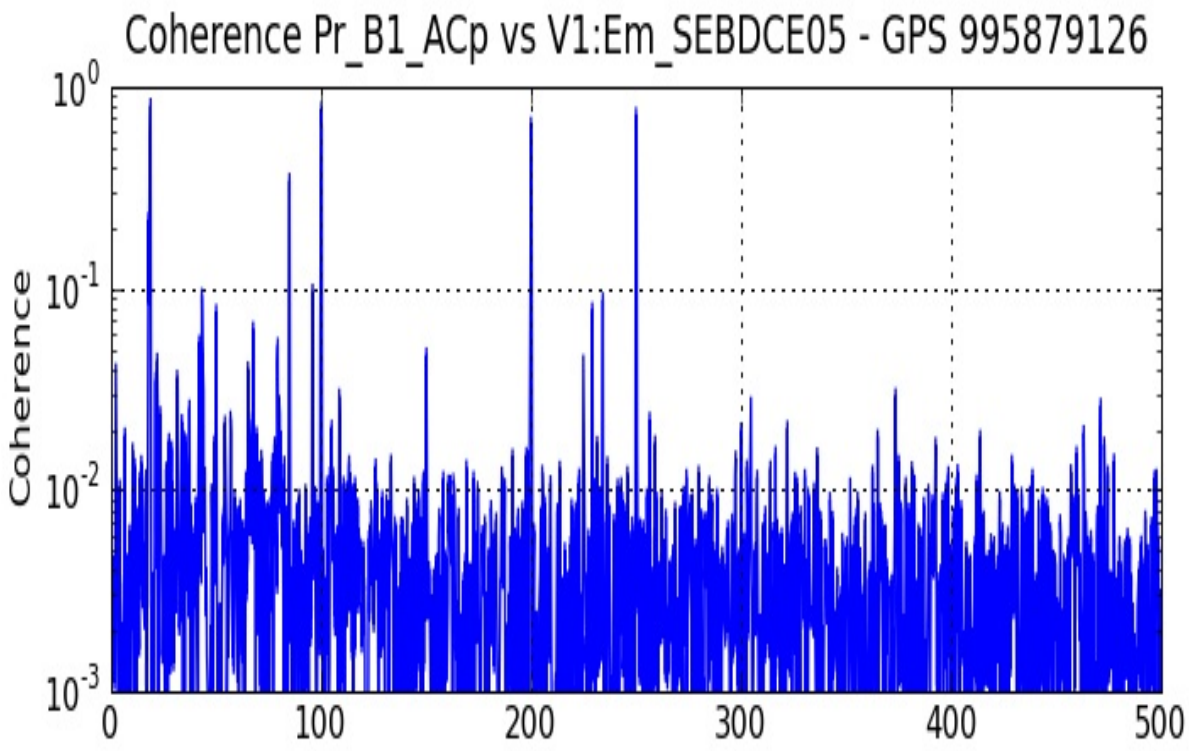

FIG. 3: A plot (coherence vs. frequency) showing the amount of coherence between the dark fringe (Pr_B1_ACp) and a seismometer (V1:Em_SEBDCE05) located in the central building between 0 and 500 Hz on July 28, 2011. High coherence is visible at frequencies of 20, 100, 200, and 250 Hz.

B. Method of Identifying Noise Lines in VSR4

To detect noise lines in the range of 10 to 100 Hz for VSR4, I first computed the coherence of the dark fringe with about 100 environmental channels around the interferometer. I performed the coherence for one hour of science data (steady horizon around 10 Megaparsecs) starting on Tuesday, June 21, 2011 at 1:00:01 UTC (Coordinated Universal Time) with a frequency resolution of approximately 0.015 Hz. I set the threshold of coherence for a possible noise line to be 0.2. Next, I compared each frequency with a coherence of 0.2 or greater with the identified noise lines of NoEMi for VSR4. I set the threshold of NoEMi to be one percent. I then compiled all of the lines that satisfied both the coherence and NoEMi thresholds. To determine the width, amplitude, and SNR of the noise lines, I created a spectrogram of the frequencies in the dark fringe over a period of an hour (the same hour of science data as the coherence). The SNR is defined as the ratio between the amplitude of the frequency peak and the amplitude of the surrounding background noise. In the spectrogram, some strong noise lines appeared that did not satisfy both the NoEMi and coherence thresholds, and so I included these lines in the list if they had an SNR above two. The full list can be seen in Appendix A, which includes the line frequency, explanation of the source, channels for which NoEMi and the coherence find correlation with the dark fringe, and the SNR of the noise line.

C. Sources of Noise Lines

After identifying noise lines in the dark fringe, it is important to determine the sources of the noise lines in effort to eliminate the noise line, or at least decrease its strength. In attempt to identify environmental noise line sources, weekly tests were performed during VSR4, usually during scheduled maintenance periods in which the interferometer "science quality" data flag is turned off so as not to pollute data that will be used for gravitational wave searches. I will first, however, identify the noise lines not from environmental sources.

There are many noise lines between 10 and 100 Hz that are intentionally injected into the interferometer (for example at the level of the suspended mirrors) to calibrate the dark fringe signal, and hence known as calibration lines. The calibration lines are necessary to convert the dark fringe signal from power units detected by the photodiode to unitless units called the *strain* that represent the relative displacement of the test masses and length of the interferometer. The calibration lines used to tune the angular position of the mirrors (Figure 4) are at frequencies: 13.0, 13.2, 13.4, 13.6, 13.8, and 14.0 Hz. These lines are essential to keep the interferometer laser beam properly aligned.

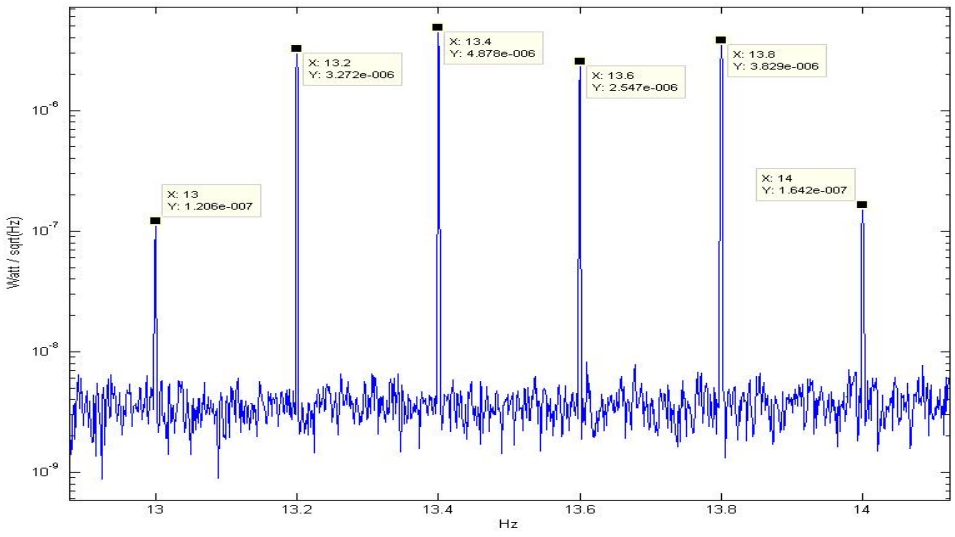

FIG. 4: A plot of the dark fringe showing the calibration lines used to align the angular position of the mirrors. These lines are intentionally injected to tune the suspension mechanism of adjusting the mirrors.

The mirror calibration lines (Figure 5) are at frequencies: 90.5, 91.0, 91.5, 92.0, 92.5. These lines are used to check that the mirrors are properly aligned with the laser beam. Additionally, there is a calibration line at frequency 9.8 Hz

to align the angles of the mirrors and two calibration lines to align the longitudinal axis of the mirrors at frequencies of 17.0 and 62.0 Hz.

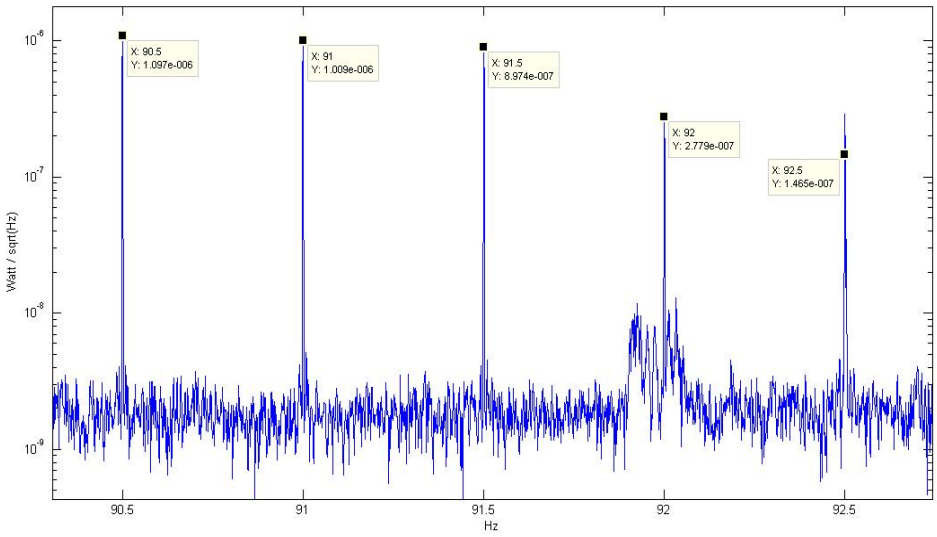

FIG. 5: The mirror calibration lines seen in the dark fringe. These lines are intentionally injected to align the mirrors with the laser beam.

There is a strong noise line at 50 Hz that is easily identifiable as the frequency at which alternating current oscillates in Italy. Since power is necessary to run the workings of the interferometer, this noise line is unavoidable. Additionally, a noise line at 100 Hz is visible in the dark fringe, which is the second order harmonic (multiple) of the 50 Hz noise line. These two noise lines are visible in Figure 6.

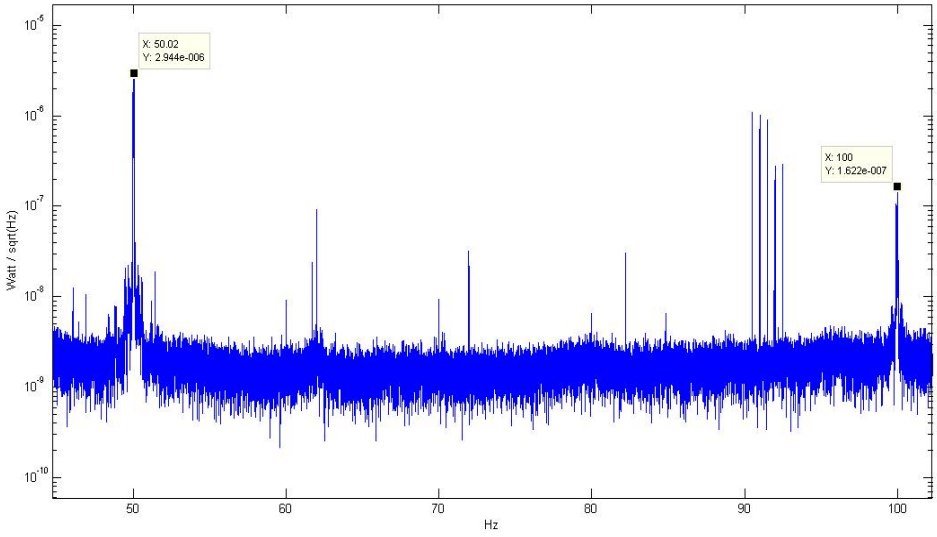

FIG. 6: A plot (amplitude vs. frequency) outlining the noise lines at 50 and 100 Hz. These lines are due to the frequency at which current oscillates in Italy.

The detection bench, which houses the sophisticated equipment to detect light in the dark fringe, has mechanical resonances between 35 and 38 Hz. It is suspected that these resonances are the result of poor performance of the seismic attenuation suspension of the detection bench and thus, the detection bench is susceptible to ground vibrations.

Therefore, the noise lines at 35.0 and 37.52 Hz are suspected resonances of the detection bench [2]. Advance Virgo intends to correct this problem by adding additional noise attenuation stages to the detection bench.

There are two line *combs* found between 10 and 100 Hz. A comb is a set of noise lines that are equally spaced, often the result of harmonics of a strong fundamental frequency. The first comb (Figure 7) is spaced at 10.0 Hz increments, starting with 10.0 Hz and ending at 100 Hz. Both the coherence and NoEMi identify this comb strongest in magnetometer channels meaning that it is most likely an electromagnetic noise. More tests are ongoing to identify the source of this noise line.

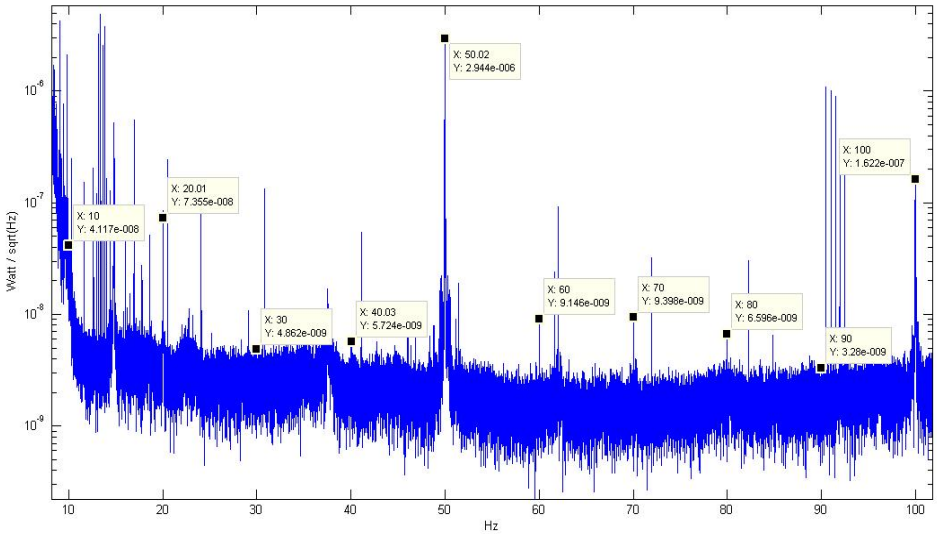

FIG. 7: A plot (amplitude vs. frequency) showing the comb of noise lines equally spaced at 10 Hz. The strong noise line at 50 Hz due to oscillating current may be the cause of this comb.

The second comb, nicknamed N-comb, is spaced by 10.28 Hz. It starts at 10.28 Hz and extends up to 82.23 Hz, as illustrated in Figure 8. N-comb is not identified by the coherence, but some harmonics of the comb are strongly identified by NoEMi, and the spectrogram of the dark fringe reveals the comb. The suspected source of N-comb is the digital clocks used to regulate data exchange among electronic devices. The digital clocks are believed to emit electromagnetic noise with similar characteristics to the N-comb frequencies. Thus, searches are ongoing in which a portable magnetic probe is placed close to suspected sources and the data is fed to a spectrum analyzer. Unfortunately, searches have yielded no conclusive results of the source.

On Wednesday, June 15, 2011, Virgo conducted a switch off test of air conditioners and fans. These devices were shut off in sequential stages in order to help indentify noise lines in the dark fringe. Since these devices are crucial to the workings of the interferometer, they can only be shut off for a small amount of time, but long enough to observe changes in noise lines. Examining a spectrogram of the Fourier transform of the dark fringe signal during the time period of the shut off reveals noise lines disappearing as certain devices are shut off, and reappearing as devices are switched back on. Using these patterns, noise line sources can be identified. The switch off test of June 15 revealed four noise line sources for the frequencies of: 16.46, 16.9, 17.78, and 18.61 Hz. Figure 9 shows that the noise line at 16.46 Hz disappeared in accordance with the shut off of the air conditioner in the injection clean room located in the main building. Figure 10 shows that the noise line at 16.9 Hz disappeared in accordance with the shut off of the air conditioner in the data acquisition room located in the central building. Figure 11 shows that the noise line at 17.78 Hz disappeared in accordance with the shut off of the fan in the detection lab located in the central building. Figure 12 shows that the noise line at 18.61 Hz also disappeared in accordance with the shut off of the fan in the detection lab. Additionally, past switch off tests have shown that the 29.08 Hz noise line is due to the air conditioner of the mode cleaner building [3].

There are many unknown noise line sources as listed in Appendix A. Investigations are ongoing to identify these noise line sources as many of them are at suspicious frequencies, suggesting tests could reveal their origins.

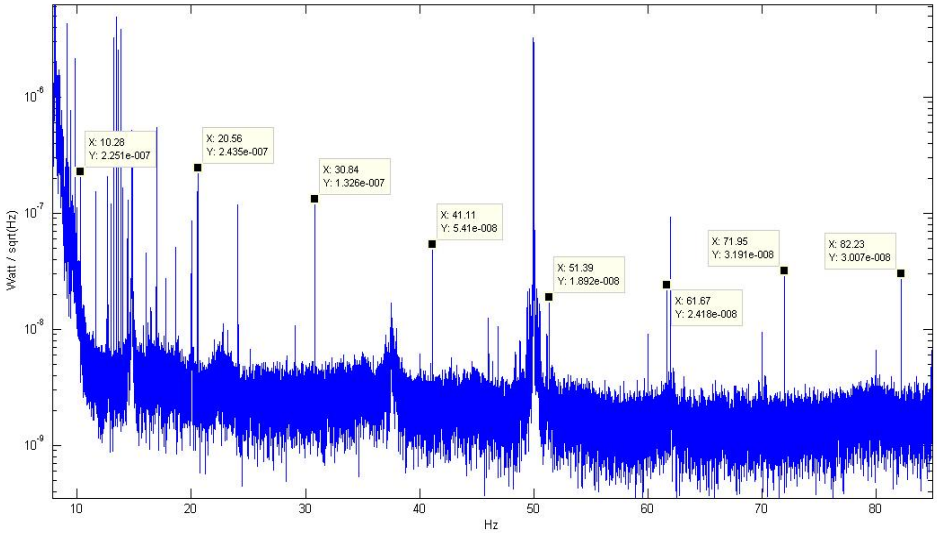

FIG. 8: The comb of noise lines equally spaced at 10.28 Hz, referred to as N-comb.

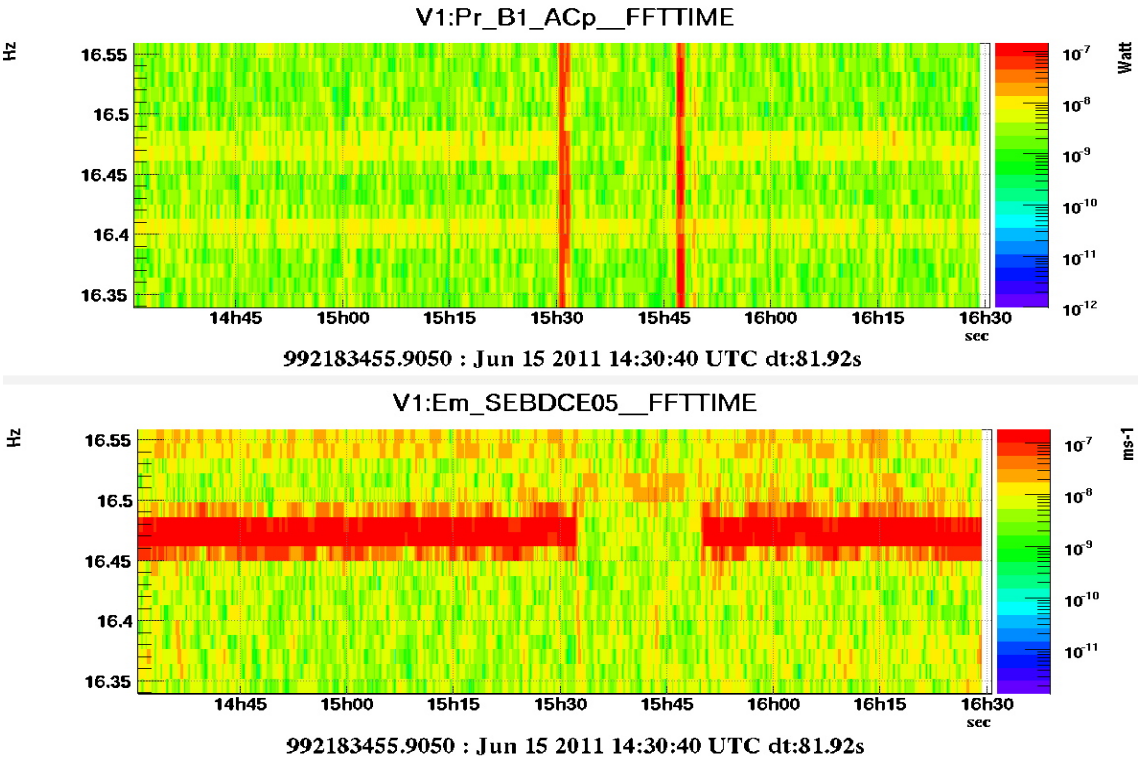

FIG. 9: A spectrogram (frequency vs. time) of the dark fringe (V1:Pr_B1_ACp) and a seismometer (V1:Em_SEBDCE05) in the central building during the shut off test reveals that the source of the noise line at 16.46 Hz is the air conditioner in the injection clean room located in the central building.

III. COOLING FANS FOR ADVANCED VIRGO

One source of noise lines is the cooling fans surrounding the interferometer. The cooling fans are necessary to dissipate heat away from the electronics, as most of the electronics must run continuously for the interferometer to

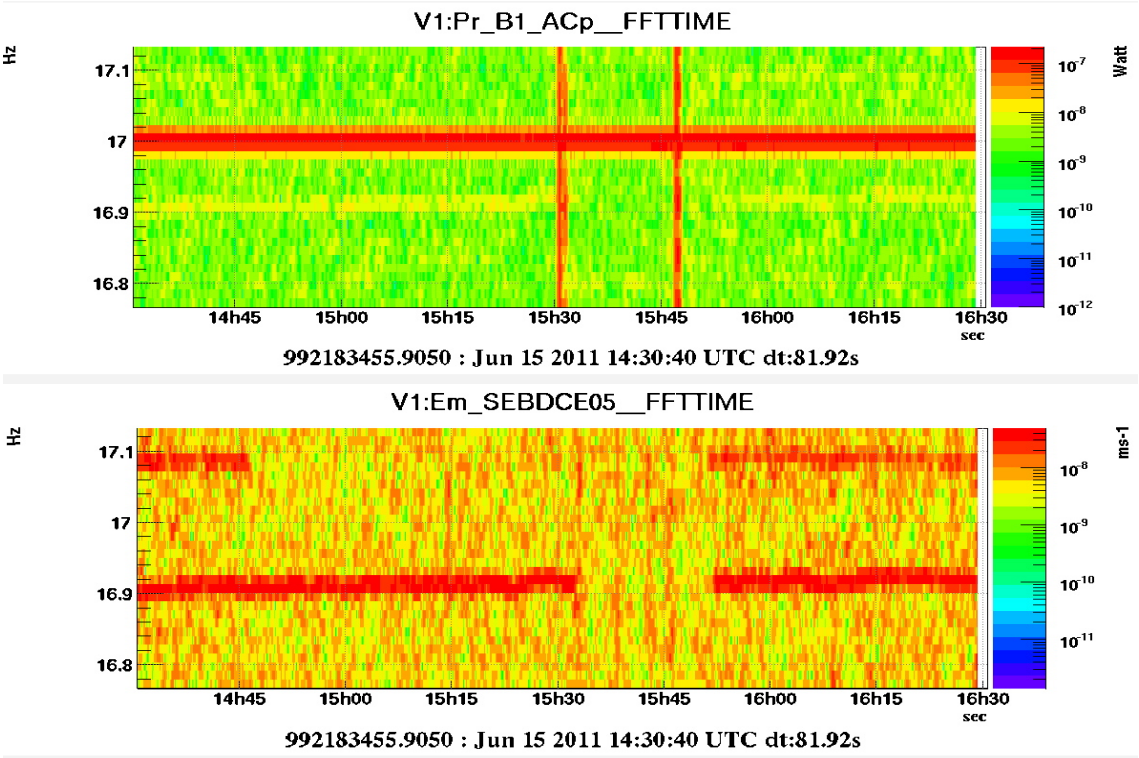

FIG. 10: A spectrogram (frequency vs. time) of the dark fringe (V1:Pr_B1_ACp) and a seismometer (V1:Em_SEBDCE05) in the central building during the shut off test reveals that the source of the noise line at 16.9 Hz is the air conditioner in the data acquisition room located in the central building.

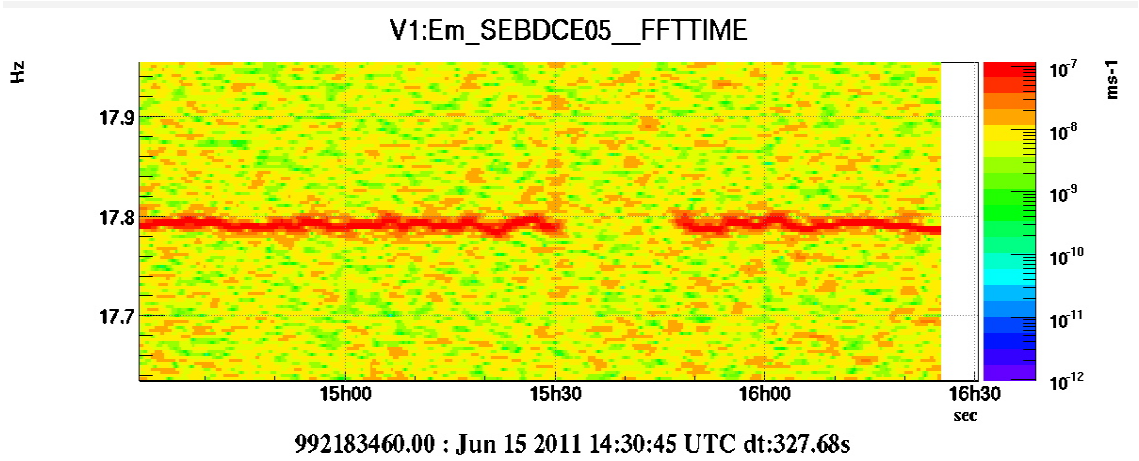

FIG. 11: A spectrogram (frequency vs. time) of a seismometer (V1:Em_SEBDCE05) in the central building during the shut off test reveals that the source of the noise line at 17.78 Hz is the fan in the detection lab located in the central building.

work properly. The motors of the cooling fans rotate at a fixed frequency, which produces a pressure wave that can cause vibrations within the interferometer at the same frequency as the fan motor. The fan noise can couple into the interferometer detector signal and produce noise lines in the dark fringe. Most of the fan motors are between 10 and 60 Hz, which is also the frequency range of many known pulsars, including the Vela and Crab. Thus, eliminating or reducing the noise from cooling fan motors could greatly increase the sensitivity around such pulsars. The maximal noise from cooling fans tolerated for Advanced Virgo is significantly less than for VSR4, and so new fans and/or new fan configurations will need to be implemented for Advanced Virgo. In anticipation for these changes, I tested five different fans whose specifications can be seen in Table I.

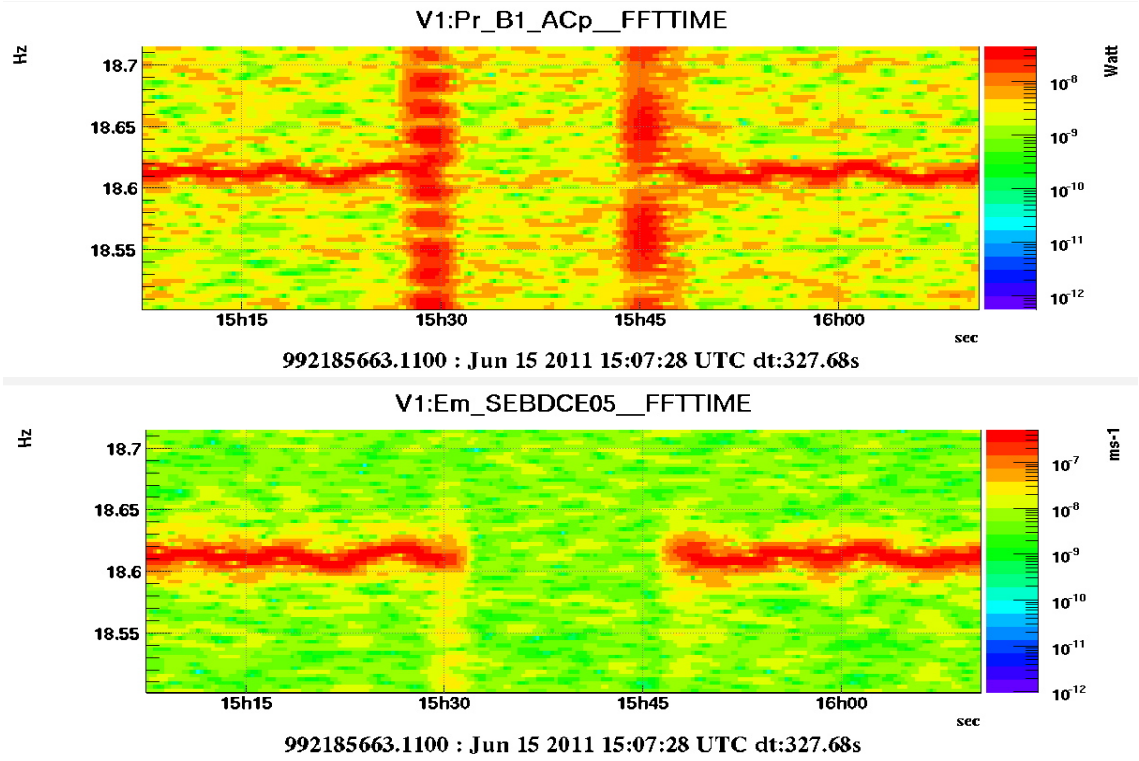

FIG. 12: A spectrogram (frequency vs. time) of the dark fringe (V1:Pr_B1_ACp) and a seismometer (V1:Em_SEBDCE05) in the central building during the shut off test reveals that the source of the noise line at 18.61 Hz is the fan in the detection lab located in the central building.

TABLE I: Fan Specifications

Fan	Bearing Type	Speed (RPM/Hz)	Noise (dBa)	Weight (g)	Dimensions (mm^3)
EbmPapst 3956L	Sintec	1550 / 25.8	24	280	92 x 92 x 25
EbmPapst 4890N	Sintec	1550 / 25.8	25	540	119 x 119 x 38
Papst 4650N	Sintec	2650 / 44.2	46	550	119 x 119 x 38
Sunon DP203A	Ball	2225 / 37.1	38	550	120 x 120 x 38
Sunon DP203AT	Ball	1800 / 30	38.5	330	119 x 119 x 25

A. Experimental Setup

I performed measurements of the five fans in the north tunnel arm of the Virgo interferometer at about 100 meters north of the 1500 North Lab on Friday, June 17, 2011 between 13:00 and 15:00 UTC. The test location was chosen after comparing the background noise in several different places around Virgo. The background noise inside the north tunnel arm was found to be the lowest, allowing for the highest SNR for the test measurements. To measure the acoustic noise from each fan, I used a microphone (Bruel and Kjaer model 4190) positioned 30 centimeters behind each fan, opposite to the direction of the fan's air flux (direct air flux from the fan on the microphone would cause additional noise). Each fan was suspended with wire from a small tower to seismically decouple the fan from its support in effort to eliminate possible acoustic noise from the vibration of the support. I then used a spectrum analyzer (Ono Sokki) to read the data from the microphone and convert the microphone signal into sound pressure for a frequency range of 0 to 2000 Hz. I made six measurements in total - one for each fan and one for the background noise.

B. Results

To evaluate the performance of each fan, I calculated the root mean square of the sound pressure, p_{rms}, which is defined as:

$$p_{rms} = \sqrt{\sum_{i=10Hz}^{2000Hz} {a_i}^2 * \delta f} \tag{3.1}$$

where a_i is the amplitude of the fan acoustic noise at frequency bin i minus the amplitude of the background (amplitude is in units of Pascals per square root of Hz) and δf is the bin width of the frequency spectrum. To compare the amount of acoustic noise emitted by a fan relative to the air flow it produces, I divided the sound pressure by the air flow - the lower this value is, the better the performance of the fan. Table II shows the results, listed in descending order of performance. Note that air flow is in units of cubic feet per minute (CFM).

TABLE II: Fan Results

Fan	p_{rms} (Pascals)	Air Flow (CFM)	p_{rms} / Air Flow
EbmPapst 4890N	0.0024	47.1	5.10E-05
Sunon DP203AT	0.0056	50.5	1.11E-04
Sunon DP203A	0.0085	75	1.13E-04
EbmPapst 3956L	0.0029	18.25	1.59E-04
Papst 4650N	0.0176	94.2	1.87E-04

Table II indicates that the fan EbmPapst 4890 performed best - that is, it emits the least amount of acoustic noise relative to the amount of air flow it produces. It is significantly less noisy than fan Papst 4650N, which is similar to the fans used for past Virgo scientific runs and currently for VSR4; but EbmPapst 4890 produces only half of the air flow of Papst 4650N. Figure 13 compares the sound pressure of EbmPapst 4890, Papst 4650, and the background noise from 10 to 1000 Hz. The plot clearly indicates that EbmPapst 4890 produces significantly less noise than Papst 4650N at frequencies greater than 100 Hz. The peaks visible in EbmPapst 4890 and Papst 4650N but not seen in the background noise are most likely the fundamental frequencies of the fan motors and its harmonics.

The results show that there are other fans that produce significantly less noise than the current fans being used for VSR4, but the ones tested also produce less air flow. More tests need to be conducted before determining the best fans for Advanced Virgo. Most importantly, the necessary amount of air flow for each vacuum rack must be determined in order to know how powerful the fans must be. One plausible option is to use larger fans that operate at frequencies lower than 10 Hz but produce similar air flows to the current VSR4 fans. Since the sensitivity below 10 Hz is much worse (due to the seismic wall) than above 10 Hz, it would be better to deterioate sensitivity which is already spoiled, instead of good sensitivity.

IV. CONCLUSION

Virgo has an extraordinary opportunity to detect the first ever gravitational wave with the significant improvement in detector sensitivity expected in Advanced Virgo; however, no experiment is perfect. External sources will always produce noise lines that deteriorate the detector sensitivity. It is important to continue identifying the sources of noise lines in VSR4 so that the necessary steps can be taken to avoid these noise lines in Advanced Virgo. The noise line identification tools, NoEMi and coherence, play a vital role in detecting noise lines and identifying their sources. Improving the detector sensitivity is not the outcome of mitigating one noise line source, but rather the combination of mitigating numerous sources. Less noisy cooling fans is just one example of the many modifications that Advanced Virgo will undergo to achieve better detector sensitivity.

Acknowledgments

I would like to thank the National Science Foundation for funding the IREU program in gravitational-wave physics that enabled me to spend the months of June and July 2011 performing the experiments described in this paper, and the University of Florida for putting together the IREU program and organizing my trip. In particular, I must thank

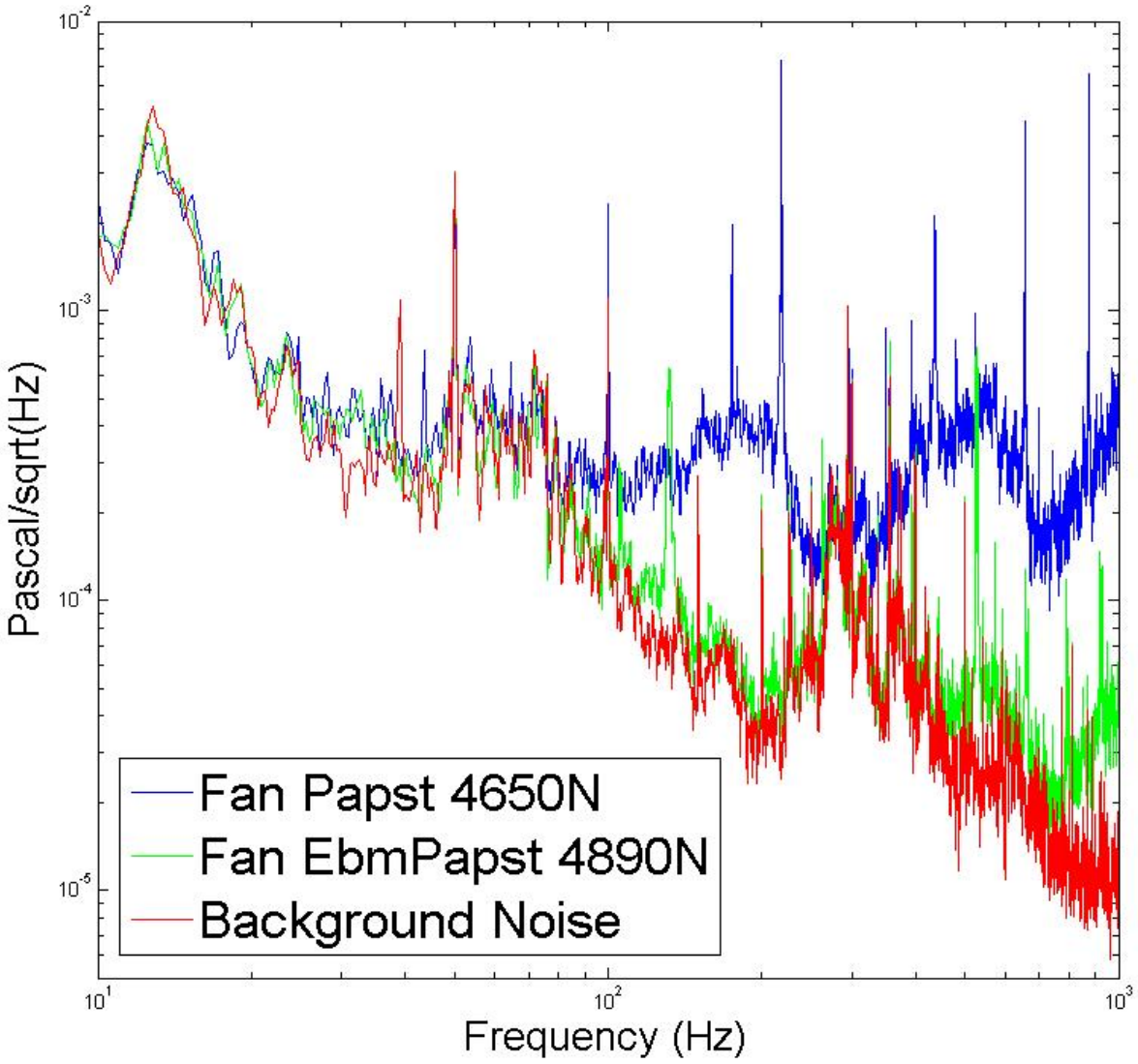

FIG. 13: A log-log plot (amplitude vs. frequency) comparing the acoustic noise for the fans Papst4650N and EbmPapst 4890, and the background noise of the measurement environment.

Professors Bernard Whiting and Guido Mueller, and Kristin Nichola. I would also like to thank Virgo and EGO (European Gravitational Observatory) for letting me partake in their extraordinary experiment, especially Dr. Irene Fiori who served as my mentor but acted as my friend. In addition, I must thank Nelson Christensen of Carleton College for first introducing me to gravitational wave physics. And, of course, my parents and family for their love and support in everything I do.

[1] Eric D. Black and Ryan N. Gutenkunst. *An introduction to signal extraction in interferometric gravitational wave detectors.* American Journal of Physic, Volume 71, Number 4, April 2003. 365–378.
[2] Virgo Collaboration, *The Virgo Data Quality*, Paper in Preparation.
[3] Virgo Webpage. https://wwwcascina.virgo.infn.it/.

Appendix A

TABLE III: VSR4 Noise Lines from 10 - 100 Hz

$Frequency(Hz)$	*Explanation*	$Noemi(> 1\%)$	$Coherence(> 0.2)$	SNR
9.8	Calibration	Em_SEBDNE02 (4.3%) Em_ACBDNE01 (3.4%)	None	33
9.95	Unknown	Em_ACBDNE01 (3.6%) Em_MABDNE01 (2.9%) Em_SE_CryoT (2.9%) Em_MABDCE01 (2.9%) Em_MABDWE01 (2.2%) Em_SEBDNE02 (1.4%)	None	5
10.28	N-Comb	Em_ACBDNE01 (4.3%)	None	19
11.63	Unknown	Em_ACBDNE01 (14.0%) Em_MABDMC02 (11.0%) Em_ACTCSNI (1.0%)	None	34
12.63	Unknown	Em_MABDMC02 (9.4%) Em_SE_CryoT (2.4%)	None	40
12.72	Unknown	Em_MABDMC02 (3.5%) Em_SE_CryoT (2.7%)	None	4
13	Calibration	Em_MABDMC02 (17.5%) Em_ACBDCE01 (1.5%)	None	37
13.2	Calibration	Em_MABDMC02 (1.0%)	None	1009
13.4	Calibration	Em_SEBDWE01 (42.0%) Em_MABDWE01 (40.5%) Em_ACBDWE01 (17.5%)	None	1134
13.6	Calibration	Em_ACTCSNI (1.9%)	None	739
13.8	Calibration	Em_ACBDCE01 (8.0%) Em_ACTCSNI (5.0%) TCS_NI_Power (3.0%) Em_MABDCE01 (1.3%)	None	793
14.0	Calibration	Em_MABDCE01 (37.3%) Pr_power50 (9.8%) Em_ACTCSNI (3.8%) Em_ACBDCE01 (3.2%) Em_MABDNE01 (1.4%)	None	31
14.42	Unknown	Em_ACBDWE01 (22.1%) Em_SEBDNE02 (9.0%) Em_MABDCE01 (7.2%) Em_MABDNE01 (4.9%) Em_SEBDWE01 (4.5%) Em_SETCSWI01 (1.4%)	None	19
14.78	Unknown	Em_SEDBDL03 (43.7%) Em_SE_EIB_04 (14.3%) Em_IPSCB_50Hz (14.0%) Em_MABDCE01 (10.9%) Em_SETCSNI02 (1.8%) Em_SETODE01 (1.2%) Em_SE_LB_04 (1.2%)	None	39

Frequency(Hz)	*Explanation*	*Noemi*($> 1\%$)	*Coherence*(> 0.2)	*SNR*
14.87	Unknown	Em_MABDNE01 (3.3%) Em_MABDCE01 (1.3%)	None	23
16.0	Unknown	Em_MABDCE01 (45.3%) Em_MABDNE01 (2.2%) Em_MABDWE01 (1.0%)	Em_MABDCE02 (0.27) Em_MABDCE01 (0.23)	5
16.23	Unknown	Em_MABDMC02 (36.8%) Em_MABDWE01 (2.1%) Em_MABDNE01 (1.1%) Em_SEBDWE01 (1.1%)	None	2
16.46	Central Building Air Conditioner injection Clean Room	Em_SETODE01 (8.6%) Em_SE_CryoT (8.5%) Em_AC_EIB (8.4%) Em_SE_EIB_04 (8.4%) Em_SE_BrewINJ (8.4%) Em_SEBDCE01 (8.3%) Em_SETCSNI02 (8.3%) Em_SETCSWI01 (8.3%) Em_SEBDCE08 (8.2%) Em_SEDBDL03 (7.2%) Em_SE_LB_04 (6.6%) Em_SEBDCE06 (4.7%)	Em_SE_EIB_04 (0.73) Em_SEBDCE09 (0.73) Em_SEBDCE08 (0.73) Em_SEBDCE07 (0.73) Em_SEBDCE11 (0.73) Em_SEBDCE10 (0.73) Em_SEBDCE12 (0.73) Em_SETCSWI02 (0.73) Em_SEBDCE05 (0.73) Em_SEBDCE14 (0.73) Em_SETCSWI01 (0.72) Em_SETOWT01 (0.72) Em_SEBDCE15 (0.72) Em_SEBDCE02 (0.72) Em_SETOIN01 (0.72) Em_SE_BrewINJ (0.72) Em_SE_LB_04 (0.72) Em_SETOPR01 (0.72)	3
16.9	Central Building Air Conditioning Data Acquisition Room	Em_SETCSWI01 (10.0%) Em_SETCSNI02 (10.0%) Em_SE_BrewINJ (10.0%) Em_SEBDCE06 (9.5%) Em_SEBDCE08 (9.5%) Em_MABDCE01 (9.5%) Em_SE_EIB_04 (9.3%) Em_SEDBDL03 (8.8%) Em_SE_LB_04 (8.4%) Em_ACBDCE01 (7.6%) Em_ACTCSNI (3.1%) Em_ACBDWE01 (2.0%) Em_IPSCB_50Hz (1.6%)	Em_SEBDCE08 (0.81) Em_SEBDCE15 (0.81) Em_SEBDCE07 (0.81) Em_SETOIN01 (0.81) Em_SE_BrewINJ (0.8) Em_SETCSWI01 (0.8) Em_SEBDCE06 (0.8) Em_SETCSWI03 (0.8) Em_SEBDCE04 (0.79) Em_SEBDCE05 (0.79) Em_SEBDCE09 (0.79) Em_SETCSNI02 (0.79) Em_SETCSNI03 (0.78) Em_SEBDCE03 (0.77) Em_SETCSWI02 (0.77) Em_SETCSNI01 (0.76) Em_SETONT01 (0.75) Em_SEBDCE11 (0.73) Em_SE_LB_04 (0.73) Em_SEBDCE10 (0.72) Em_SETCSNI03 (0.72) Em_SEBDCE13 (0.71)	5
17.0	Calibration	Em_ACBDWE01 (4.6%) Em_SE_BrewINJ (2.2%) Em_SE_EIB_04 (2.2%) Em_SETODE01 (1.9%) Em_SE_CryoT (1.9%)	None	94

Frequency(Hz)	*Explanation*	*Noemi*($> 1\%$)	*Coherence*(> 0.2)	*SNR*
17.78	Central Building Fan Detection Lab	Em_SE_BrewINJ (10.7%) Em_SETCSNI02 (10.6%) Em_SE_EIB_04 (10.5%) Em_SEDBDL03 (10.2%) Em_SEBDCE08 (10.2%) Em_SEBDCE01 (9.5%) Em_SEBDCE06 (9.2%) Em_SETCSWI01 (8.8%) Em_SE_LB_04 (8.1%) Em_SE_CryoT (4.4%) Em_ACBDNE01 (4.1%) Em_ACBDWE01 (1.4%) Em_MABDNE01 (1.1%)	Em_SETOIN01 (0.88) Em_SE_BrewINJ (0.88) Em_SEBDCE06 (0.88) Em_SEBDCE04 (0.87)	6
18.61	Central Building Fan Detection Lab	Em_SETODE01 (7.8%) Em_SE_EIB_04 (7.7%) Em_SEDBDL03 (7.7%) Em_SE_CryoT (7.6%) Em_SETCSWI01 (7.6%) Em_SEBDCE01 (7.6%) Em_SE_BrewINJ (7.6%) Em_AC_EIB (7.6%) Em_SETCSNI02 (7.5%) Em_SEBDCE08 (7.4%) Em_ACBDCE01 (6.8%) Em_SE_LB_04 (6.6%) Em_SEBDCE06 (5.0%) Em_ACTCSNI (4.6%)	Em_SEBDCE10 (0.97) Em_SEBDCE07 (0.97) Em_SEBDCE08 (0.97) Em_SEBDCE12 (0.97) Em_SE_EIB_04 (0.97) Em_SEBDCE13 (0.97) Em_SEBDCE09 (0.97) Em_SEBDCE03 (0.97) Em_SETCSWI01 (0.97) Em_SEBDCE05 (0.97) Em_SE_BrewINJ (0.97) Em_SETOWT01 (0.97) Em_SETOIN01 (0.97) Em_SEBDCE01 (0.97) Em_SEBDCE04 (0.97) Em_SEBDCE15 (0.97) Em_SETCSWI02 (0.97) Em_SETCSWI03 (0.97) Em_SETCSNI03 (0.97) Em_SEDBDL03 (0.97)	13
20.0	T-comb	Em_MABDNE01 (31.3%) Em_MABDCE01 (31.3%) Em_MABDWE01 (30.5%) Em_SE_CryoT (2.5%) Em_MABDMC02 (2.0%)	None	18
20.56	N-Comb	Em_ACBDNE01 (25.3%) Em_ACBDWE01 (11.1%) Em_SE_CryoT (2.7%)	None	67
24.03	Unknown	Em_MABDMC02 (15.4%) Em_AC_EIB (5.3%) Em_SEBDNE02 (2.4%)	None	42
29.08	Air Conditioner in Mode Cleaner Building	Em_MABDMC02 (40.4%) Em_ACBDWE01 (4.0%) Em_SEBDWE01 (4.0%) Em_IPSCB_50Hz (4.0%)	Em_SEBDMC01 (0.77) Em_SEBDMC02 (0.74) Em_SEQMC1 (0.73) Em_SEQMC3 (0.73) Em_SEBDMC03 (0.73) Em_SETOMC01 (0.68) Em_SEQMC2 (0.34) Em_MABDMC02 (0.3) Em_ACBDMC01 (0.25)	3

Frequency(Hz)	*Explanation*	*Noemi*($> 1\%$)	*Coherence*(> 0.2)	*SNR*
30.0	T-comb	Em_MABDWE01 (32.9%) Em_MABDNE01 (32.2%) Em_MABDCE01 (32.1%) Em_SEBDWE01 (1.5%)	Em_MABDNE01 (0.25) Em_MABDNE02 (0.23) Em_MABDWE03 (0.2) Em_MABDWE01 (0.2) Em_MABDCE02 (0.19) Em_MABDCE01 (0.19) Em_MABDNE03 (0.16)	2
30.84	N-Comb	Em_SEDBDL03 (31.4%) Em_SEBDCE01 (29.3%) Em_SETODE01 (22.8%) Em_IPSCB_50Hz (4.0%) Em_SEBDCE06 (3.4%) Em_SEBDCE08 (1.8%) Em_SETCSNI02 (1.3%) Em_SE_CryoT (1.2%)	None	44
35.0	Suspected Resonance of the Suspended Detection Bench	Em_IPSCB_50Hz (6.5%) Em_SEBDCE08 (1.2%) Em_ACTCSNI (1.2%)	Em_SEBDCE15 (0.55) Em_SETODE01 (0.5) Em_SEBDCE13 (0.5) Em_SE_CryoT (0.39) Em_ACBDCE01 (0.34) Em_ACTCSNI (0.3) Em_SEBDCE04 (0.27) Em_SEBDCE03 (0.27) Em_SEBDCE02 (0.26) Em_SEBDCE05 (0.25) Em_SETOPR01 (0.24) Em_ACDBDL01 (0.22) Em_SEBDCE06 (0.2) Em_SEBDCE01 (0.19) Em_SETOIN01 (0.19) Em_SE_BrewINJ (0.15)	2
37.52	Suspected Resonance of the Suspended Detection Bench	Em_SEBDWE01 (8.8%) Em_SETODE01 (6.6%) Em_SEBDNE02 (4.2%) Em_IPSCB_50Hz (4.2%) Em_SE_BrewINJ (3.9%) Em_SE_LB_04 (2.1%) Em_MABDNE01 (1.8%) Em_AC_EIB (1.2%) Em_MABDCE01 (1.2%)	Em_SEBDCE15 (0.76) Em_SETODE01 (0.71) Em_SEBDCE13 (0.64) Em_SEBDCE03 (0.49) Em_SEBDCE01 (0.45) Em_SEBDCE02 (0.28) Em_SE_CryoT (0.26) Em_SEBDCE05 (0.25)	4
40.0	T-comb	Em_MABDWE01 (37.7%) Em_MABDCE01 (35.4%) Em_SE_BrewINJ (17.3%) Em_SEBDWE01 (4.2%) Em_ACTCSNI (2.1%) Em_MABDNE01 (1.9%)	Em_MABDNE02 (0.27) Em_MABDCE01 (0.26) Em_MABDCE02 (0.23) Em_MABDWE01 (0.19) Em_MABDCE03 (0.16)	2
41.11	N-Comb	None	None	21
46.02	Unknown	Em_SEBDWE01 (4.7%) Em_ACBDNE01 (2.1%)	None	6
46.38	Unknown	None	None	2
46.86	Unknown	None	None	5
48.4	Unknown	None	Em_IPSMC_50Hz (0.71) Em_IPSCB_50Hz (0.7)	3
48.8	Unknown	None	None	3

Frequency(Hz)	*Explanation*	*Noemi*($> 1\%$)	*Coherence*(> 0.2)	*SNR*
50.0	Alternating Current	Pr_power50 (4.8%) Em_SETODE01 (4.8%) Em_IPSCB_50Hz (4.8%) Em_MABDWE01 (4.8%) Em_MABDMC02 (4.8%) Em_ACTCSNI (4.7%) Em_MABDNE01 (4.7%) Em_SEDBDL03 (4.7%) Em_MABDCE01 (4.7%) Em_AC_EIB (4.7%) Em_SETCSWI01 (4.7%) Em_SEBDCE01 (4.7%) Em_SEBDWE01 (4.7%) Em_SEBDCE08 (4.6%) TCS_WI_Power (4.5%) TCS_NI_Power (4.5%) Em_SE_BrewINJ (4.3%) Em_SE_LB_04 (4.1%) Em_SE_EIB_04 (3.8%) Em_SETCSNI02 (3.5%)	All Channels	498
51.39	N-Comb	None	None	9
60.0	T-comb	Em_MABDWE01 (42.8%) Em_MABDCE01 (42.2%) Em_MABDMC02 (11.1%) Em_IPSCB_50Hz (1.0%)	Em_MABDCE01 (0.68) Em_MABDCE02 (0.64) Em_SEBDCE02 (0.62) Em_MABDCE03 (0.6) Em_MABDNE02 (0.15) Em_SETOPR01 (0.15)	5
61.67	N-Comb	None	None	11
62.0	Calibration	Em_SETODE01 (27.9%) Em_SE_CryoT (15.6%) Em_SEBDCE08 (10.7%)	None	39
70	T-comb	Em_MABDCE01 (34.0%) Em_MABDNE01 (33.5%) Em_MABDWE01 (31.5%)	Em_MABDCE01 (0.58) Em_MABDNE02 (0.57) Em_SEBDCE02 (0.57) Em_MABDCE02 (0.56) Em_MABDCE03 (0.45) Em_MABDNE01 (0.34) Em_MABDWE03 (0.17)	5
71.95	N-Comb	Em_SE_LB_04 (5.2%) Em_MABDWE01 (2.8%) Em_IPSCB_50Hz (1.8%) Em_SETODE01 (1.6%)	None	21
80.0	T-comb	Em_MABDWE01 (48.6%) Em_MABDCE01 (40.7%) Em_MABDNE01 (7.8%) TCS_WI_Power (1.4%)	Em_MABDCE02 (0.37) Em_SEBDCE02 (0.33) Em_MABDNE02 (0.33) Em_MABDWE01 (0.31) Em_MABDCE01 (0.3) Em_MABDCE03 (0.29) Em_MABDNE01 (0.19) Em_MABDWE03 (0.18)	3
82.23	N-Comb	Em_ACBDNE01 (6.1%)	None	18

Frequency(Hz)	*Explanation*	*Noemi*($> 1\%$)	*Coherence*(> 0.2)	*SNR*
84.84	Unknown	Em_SE_CryoT (20.8%) Em_SE_BrewINJ (20.7%) Em_SEBDCE06 (17.0%) Em_SE_LB_04 (16.5%) Em_ACTCSNI (14.6%) Em_ACBDCE01 (7.1%) Em_SEDBDL03 (1.8%)	Em_SETOPR01 (0.83) Em_SEBDCE04 (0.83) Em_SEBDCE06 (0.83) Em_SE_BrewINJ (0.83) Em_SEBDCE05 (0.83) Em_SETOBS01 (0.83) Em_SETOWT01 (0.83) Em_SEBDCE15 (0.83) Em_SEBDCE13 (0.82) Em_SETONT01 (0.81) Em_SETCSNI03 (0.77) Em_SEBDCE12 (0.76) Em_SE_CryoT (0.71) Em_SEBDCE11 (0.69) Em_SETOIN01 (0.68) Em_SEBDCE10 (0.57) Em_SE_LB_04 (0.55) Em_ACTCSNI (0.54) Em_SEBDCE03 (0.53) Em_SETCSNI01 (0.52)	3
90.0	T-comb	Em_MABDWE01 (38.1%) Em_MABDNE01 (37.2%) Em_SE_LB_04 (15.0%) Em_SE_BrewINJ (5.9%) Em_MABDCE01 (1.8%) Em_SE_CryoT (1.2%)	Em_MABDNE01 (0.28) Em_MABDNE02 (0.27) Em_MABDCE02 (0.23) Em_MABDCE01 (0.18)	2
90.5	Photon Calibration (North Input)	Em_IPSCB_50Hz (3.7%) Em_SE_BrewINJ (3.2%)	None	518
91.0	North End Calibration	Em_SE_BrewINJ (1.0%)	None	571
91.5	West End Calibration	None	None	540
92.0	Beam Splitter Calibration	m_IPSCB_50Hz (33.1%) TCS_NI_Power (4.8%) Em_ACBDNE01 (2.3%) Em_SETCSNI02 (1.6%) Em_SE_LB_04 (1.4%) Em_ACTCSNI (1.0%)	None	127
92.5	N-Comb and Power Recycling Calibration	Em_SETCSNI02 (10.6%) Em_ACTCSNI (10.5%) Em_SETCSWI01 (7.9%) TCS_NI_Power (4.0%) Em_SEBDCE06 (3.0%) Em_SE_LB_04 (1.0%)	None	143
100	Alternating Current	Em_SETODE01 (4.1%) Em_MABDWE01 (4.1%) Pr_power50 (4.1%) Em_IPSCB_50Hz (4.0%) Em_SE_EIB_04 (4.0%) Em_MABDMC02 (4.0%) Em_MABDNE01 (4.0%) Em_SEDBDL03 (4.0%) Em_AC_EIB (4.0%) Em_SE_BrewINJ (4.0%) Em_ACTCSNI (4.0%) Em_ACBDCE01 (3.9%) Em_MABDCE01 (3.9%) Em_SEBDNE02 (3.9%) Em_SETCSWI01 (3.9%) TCS_WI_Power (3.8%) Em_SETCSNI02 (3.8%)	Em_MABDNE01 (0.93) Em_MABDCE01 (0.73) Em_MABDCE03 (0.71) Em_SEBDWE01 (0.69) Em_SEQMC1 (0.66) Em_SEBDWE02 (0.64) Em_SEBDCE01 (0.6) Em_MABDNE03 (0.57) Em_SEQMC3 (0.55) Em_MABDNE02 (0.53) Em_SEDBDL03 (0.53) Em_SEBDWE03 (0.51) Em_MABDCE02 (0.51) Em_SEQMC2 (0.49) Em_ACTCSNI (0.49) Em_SEBDNE03 (0.48) Em_SETCSWI01 (0.48)	67